Construction and Building Materials 159 (2018) 316–328

Contents lists available at ScienceDirect

Construction and Building Materials

journal homepage: www.elsevier.com/locate/conbuildmat

Comparative study of the mechanical and thermal properties of lightweight cementitious composites

Adam L. Brooks, Hongyu Zhou *, Dominic Hanna

Civil and Environmental Engineering, University of Alabama in Huntsville, Huntsville, AL 35899, United States

HIGHLIGHTS

- Mechanical and thermal properties of cementitious composites with lightweight fillers were studied.
- The effects of filler type, particle size, and shell properties were systematically investigated.
- Microstructures and failure mechanisms were examined.
- Analytical approach was proposed to calculate material thermophysical properties.

ARTICLE INFO

Article history:
Received 8 August 2017
Received in revised form 23 October 2017
Accepted 25 October 2017

Keywords:
Light-weight cementitious composite
Particulate aggregates
Mechanical properties
Thermal properties
Microstructural analysis

ABSTRACT

Lightweight concrete and cementitious composites are increasingly studied by researchers due to their advantageous performance in reducing structural load and building's operational energy consumption. In this research, a comprehensive and thorough study was carried out to investigate the effects of different lightweight fillers on both the mechanical and thermal properties of lightweight cementitious composites, or LWCCs. Four different types of lightweight fillers (LWFs) including expanded polystyrene (EPS) beads, dry-expanded thermoplastic microspheres (ETM), hollow glass microspheres (HGM), and fly ash cenospheres (FACs) are studied in conjunction with various particle sizes, shell wall thickness, and proportions. Both mechanical and thermophysical properties were tested for these LWCCs after 28-day curing. The results indicated that the thermal property of LWCC is mostly governed by the volume fraction of LWFs and it can be accurately predicted by the Felske equation, whereas the mechanical properties are heavily affected by the type and property of LWF particles included. It was revealed that most fly ash cenospheres (FAC) and hollow glass microspheres (HGM) with higher density are suitable for producing LWCC materials that may be used for structural applications, whereas lower density HGMs and LWFs with soft polymer shell are more suitable for nonstructural thermal insulating components.

1. Introduction

The use of lightweight concretes (LWCs) in building structures brings twofold advantages: first, the use of LWC reduces structural weight and the dead load acting on the structures which would lead to smaller structural members and foundation size [1]; secondly, they have lower thermal conductivity than normal weight concrete which will in turn reduce building energy consumption and provide better fire resistance [2]. The reduction of a building's operational energy and the associated greenhouse gas emissions is critical for its life-time sustainability. Since energy consumed in space heating and cooling constitutes a major portion of a building's total energy consumption [3], construction materials with low thermal conductivity can effectively reduce the heat exchanged between a building's interior space and the outside environment.

Traditionally, lightweight concretes are produced by incorporating lightweight course aggregates (LWA) such as expanded perlite [4–6], shale [7–9], and expanded clay [10] into concrete. While the unit weight of these materials has been successfully achieved within the stipulated guidelines [11,12], traditional lightweight concrete and cementitious composites had lower mechanical strength and reduced performance such as impaired durability [10] and brittle failure [13]. In order to circumvent the drawbacks presented by traditional lightweight aggregate concrete, more recently, millimeter and micrometer size lightweight functional fillers (LWFs) including expanded polystyrene beads, expandable thermoplastic microspheres [14], hollow glass microspheres [15–17], and fly-ash cenospheres [18–21] have been exploited to

* Corresponding author.
E-mail address: hongyu.zhou@uah.edu (H. Zhou).

https://doi.org/10.1016/j.conbuildmat.2017.10.102
0950-0618/

produce high performance LWCC for structural application in buildings. Some of the emerging LWFs are introduced herein.

1.1. LW cement mortar with EPS beads and plastic microspheres

Expanded polystyrene (EPS) beads are artificial ultra-lightweight aggregate (typical density < 30 kg/m^3 [22]) with rounded shape and smooth surface. Earlier research on expanded polystyrene (EPS) concrete incorporates millimeter-size EPS spheres into mortar or cement paste to reduce density and thermal conductivity [22]. In comparison to regular lightweight aggregate concrete (LWAC), EPS concrete has shown better workability and volume stability [23]. It has been used for the fabrication of light-weight concrete bricks [24] and even load-bearing structural components [25]. Structural elements made from EPS concrete can be fabricated at the construction site. This provides advantages over other materials such as autoclaved cellular concrete whose fabrication process has to be performed in a well-controlled environment at a prefabrication plant. On the other hand, the drawbacks of EPS concrete are also well documented including low thermal resistance (i.e., EPS combust and release toxic gas at temperature above its ignition point) and because of its very low density, EPS aggregates are prone to segregation during mixing [24]. Mechanically, EPS concrete has shown low mechanical strength and brittle failure [22].

In addition, Aglan et al. [14] incorporated micro-size hollow expandable thermoplastic microspheres (ETM) with average particle size around 35–55 μm into cement paste. Their study showed improvements in tensile strength and fracture toughness for cement pastes having 0.1–0.4 wt% of ETM.

1.2. Hollow glass microsphere (HGM) bubbles

Due to its higher crush strength, light weight, and thermally insulating features, hollow glass microsphere (HGM) bubbles have been explored as an lightweight micro-filler in cementitious binders [16]. In comparison with polymer-based lightweight aggregate such as EPS beads and ETM, glass microspheres offer advantages including high crush strength, good thermal resistance (with typical softening temperature around 650 °C), and the cement mortars containing HGMs have more predictable mechanical and thermal properties [15]. In addition, the spherical shape and smooth surface of HGM can be utilized to alter the rheological property of fresh cement mortar, which has led to their applications in oil well cement slurry [26]. However, since the chemical properties of most HGM resemble those of a soda-lime borosilicate glass, cement mortar containing HGM particles may experience some degree of alkali-silica reaction [27]. In addition, due to its smooth surface and weak bonding to cement paste binder, HGM modified cementitious materials typically exhibit lower strength and brittle failures [17].

1.3. Fly-ash cenospheres (FAC)

Fly-ash cenospheres, or FAC, are an alumino-silicate based by-product of coal combustion at thermal power plants [28]. The coal burning process in the thermal power plants produces fly ash in both solid and hollow (cenosphere) particulate forms. Most cenosphere particles have spherical shape and hollow interior covered by a thin shell with typical shell thickness of about 5–15% of its diameter. Due to its hollow structure, FAC have low particle density (400–900 kg/m^3) and low thermal conductivity. It has been used for making ultra-lightweight concrete and cementitious composite (e.g., ULCC) in recent years [18–21]. The composition of FAC is mostly compatible with cementitious binders. Due to its partial pozzolanic reactivity, together with the rougher surface of FAC, it provides good interfacial bonding within the mortar system.

Although individual researches have been conducted for each type of the aforementioned lightweight aggregates/ filler materials, there still lacks a comprehensive investigation on the mechanical and thermal performance of cementitious composites containing these emerging LWFs. Unlike most lightweight coarse aggregates with irregular shape and porous surfaces (e.g., expanded shale clay), the lightweight particulate aggregates/ fillers discussed in this paper have much smaller particle size and are mostly spherical in shape (or have a core-shell configuration). This will allow the fine-tuning of material properties by varying material parameters such as particle size, shell thickness (stiffness), and volume fraction. For this purpose, an accurate knowledge of relationships between the composition, aggregate property, and the equivalent properties of the cementitious composites is required.

In this research, a comparative study is conducted on the properties of lightweight cementitious composites (LWCCs) mixed with four types of lightweight aggregates/filler particles – i.e., EPS beads, dry-expanded plastic microspheres, hollow glass microspheres, and fly ash cenospheres. The materials' thermophysical (e.g., density, thermal conductivity) and mechanical (compressive strength) properties are investigated with respect to the particle type, size distribution, as well as their volume concentration. Key parameters governing the material thermal and mechanical properties are discussed, and the composition-property relationships are deduced from both experiment results and predictive models. The results will provide valuable insights into the quantitative design of concrete and cementitious composites containing micrometer and millimeter size lightweight particle fillers.

2. Experimental program

2.1. Material preparation and mix design

The constituent materials used for preparing the lightweight and ultra-lightweight cementitious composites in this study include ASTM Type I-II Portland cement, silica sand (*US silica*), water, superplasticizer (*Sika Corp.*), and lightweight fillers (LWF). The water to cement ratio (w/c) was selected at 0.43 for all mixtures. The mass of cement, sand, and water used for each cubic meter of the reference mortar (without LWF) are 530.64 kg/m^3, 1367.67 kg/m^3, and 228.18 kg/m^3, respectively. The LWF used in this research include expanded polystyrene (EPS) beads, expanded thermoplastic microspheres (ETM), hollow glass microspheres (HGM), and fly ash cenospheres (FAC). For each type of LWF, different particle properties (i.e., size, density, crushing strength, and volume fraction etc.) were studied with respect to their influences on the mechanical and thermophysical properties of LWCC. For each group of LWF tested herein, four LWF volume fractions (v_f) – i.e., namely 7%, 14%, 21%, and 28% of the total volume were tested and for each volume fraction the equivalent volume of regular fine aggregate (i.e., silica sand) was deducted from the mix (i.e., the amount of silica sand used for v_f = 7%, 14%, 21%, and 28% are 1138.37 kg/m^3, 937.38 kg/m^3, 715.83 kg/m^3, and 533.71 kg/m^3, respectively). The air content of fresh cement mortar was measured at 2–5% according to ASTM C185 – 15a, which does not account for the air contained within the LWF. The properties of lightweight micro-fillers (LWF) used in this research are listed in Table 1 and are briefly introduced as follows.

EPS beads and ETM

Two types of EPS beads with average particle size of 2.5 mm (noted as "medium") and 1 mm (noted as "small") are used in this

Table 1
Properties of the lightweight particle filler (LWF) materials used in this research.

Group ID#	Material	Particle size (μm)*			Wall thickness – t (μm)**	t/D_{50}	Density (g/cm^3)	Crush strength (MPa)***
		D_{10}	D_{50}	D_{90}				
EPS-M	EPS beads (2.5 mm)	–	250	–	–	–	0.013	–
EPS-S	EPS beads (1 mm)	–	100	–	–	–	0.031	–
TPMS	Thermoplastic microsphere	–	35–55	–	–	–	0.025	–
HGM K25	Hollow glass microsphere (HGM)	25	55	90	0.85	0.015	0.25	0.75
HGM S32		20	40	70	0.88	0.022	0.32	2
HGM S38HS		19	44	70	1.20	0.027	0.28	5.5
HGM H50		15	35	50	1.70	0.049	0.50	10
HGM S60		12	29	48	1.49	0.051	0.60	10
FAC E106	Fly ash cenosphere (FAC)	42.6	81.3	125.2	4.8	0.059	0.91	1.6–3.2
FAC E160		44.9	90.6	155.4	6.0	0.066	0.76	1.6–3.2
FAC E200/600		81.3	349.1	457.2	16.5	0.047	0.82	1.6–3.2

* Particle size data for the thermoplastic microspheres and hollow glass microspheres (HGM) were reported by the manufacturer. The particle size of FACs was tested using laser diffraction and those of EPS beads were analyzed using an air jet sieve.
** The wall thickness of LWF was tested using SEM microcopy where the particles are dispersed within an epoxy matrix. Then the samples were grinded and polished to expose the section of shell.
*** The crush strength was determined using an isostatic method for the tested bubbles to have 90% survival rate.

research. The particle size of EPS beads was analyzed using an air jet sieve. The densities of medium and small EPS beads were tested at 0.013 g/cm^3 and 0.031 g/cm^3, respectively. The thermoplastic microspheres are produced by *AkzoNobel* (*Expancel*™ 461 DET 40 d25) with average particle size of 35–55 μm as reported by the manufacturer's material datasheet [29]. The density of ETM particles was tested at 0.025 g/cm^3 by gas pycnometry.

Glass microsphere bubbles

Five types of hollow glass microsphere (HGM) bubbles with density ranging from 0.25 g/cm^3 to 0.6 g/cm^3 were used for the mixes. The HGMs used in this research are produced by 3 M™. The average particle densities tested by gas pycnometry for HGM K25, S32, S38HS, H50, and S60 are 0.25 g/cm^3, 0.32 g/cm^3, 0.38 g/cm^3, 0.50 g/cm^3, and 0.60 g/cm^3, respectively. The microspheres also have different particle size (in descending order), wall thickness, and isostatic crush strength as listed in Table 1. The particle sizes were tested by laser diffraction and reported by the manufacture. The isostatic crush strength refers to the pressure at which an average lot of material has 90% or higher survival [30]. The HGM H50 bubbles also have a layer of saline-epoxy coating to enhance the interfacial bonding between the glass microsphere and the cementitious matrix.

Fly-ash cenospheres (FAC)

Three types of cenospheres (*CenoStar*) with particle sizes up to 106 μm (E106), 160 μm (E160), and 600 μm (E200/600) are studied in this research. X-ray Diffraction (XRD) analysis performed on the FACs (Fig. 1(a)) indicated that the cenospheres are comprised primarily of SiO_2 and Al_2O_3, and there is a large amount of amorphous materials with small amounts of mullite and calcite. The E200/600 also contains a small amount of quartz (Fig. 1(a)). The particle size distributions were tested using a Laser Diffraction particle size analyzer (Horiba LA-950) and the results are plotted in Fig. 1(b). The particle shell thicknesses were measured using scanning electron microscopy (SEM) imaging where the particles were embedded in epoxy and ground using a Buehler EcoMet™ grinder/polisher to expose the section of the FAC shell. Fig. 1(c) presents the SEM images showing the surface morphologies of each type of FAC particles studied herein.

For testing the mechanical and thermal property of LWCC, eleven (11) groups (a total of 55 mixtures) of mortar samples were tested. For each group, five 50 mm (2-inch) by 100 mm (4-inch) cylinders were made for compression tests and three 50 mm × 50 mm × 50 mm cubic specimens were made for thermal property tests.

2.2. Thermal property test using Transient Plane Source (TPS) method

The thermal properties (i.e., thermal conductivity and volumetric heat capacity) of LWCCs were tested using the Transient Plane Source (TPS) method [31] (*HotDisk TPS-1500*). The TPS method uses a conducting pattern with negligible heat capacity acting simultaneously as the heating element and temperature sensor (e.g., the Kapton supported double spiraled nickel metal sensor as shown in Fig. 2(a)). To solve for the thermal constants of the tested material, the hot disk sensor is assumed to consist of a series of concentric ring heat sources located in an infinitely large sample. When the double spiral sensor is electrically heated, its increase in resistance is measured as a function of time:

$$R(t) = R_0[1 + \Omega(\Delta T_i + \Delta T_{avg}(\tau))] \quad (1)$$

where R_0 is the initial resistance of the sensor prior to the heating; Ω is the coefficient of resistivity; ΔT_i is a measure of the thermal contact between the sensor and the test sample, and it becomes a constant momentarily after the heating starts. The time-dependent temperature increase, $\Delta T_{avg}(\tau)$, is recorded and the thermal conductivity k and thermal diffusivity α of the tested material can be simultaneously obtained through a process of iteration. The TPS method provides a fast yet accurate method to measure thermal conductivity and thermal diffusivity of materials [32]. The test time for each measurement normally ranges from tens of seconds to several minutes, which is substantially shorter than those of steady-state test methods such as the guarded hot box (GHB) tests [33]. The TPS method can also use different sensor sizes to accommodate different sample types. The optimal sample sizes are usually determined by the material homogeneity [32].

For the TPS tests, the LWCC cubes were cut into two identical halves (50 × 50 × 22 mm), see Fig. 2(b). Then, the samples were dried in a convection oven for 24 h and cooled down to room temperature in an air-tight desiccant cabinet to prevent condensation. The TPS tests were then performed using a HotDisk TPS-1500 thermal constant analyzer according to the ISO22007-2 specifications [31]. The applicable thermal conductivity testing range of the equipment was 0.01–400 W/m K. Three repeated measurements were taken on each tested sample to ensure the consistency of the test results.

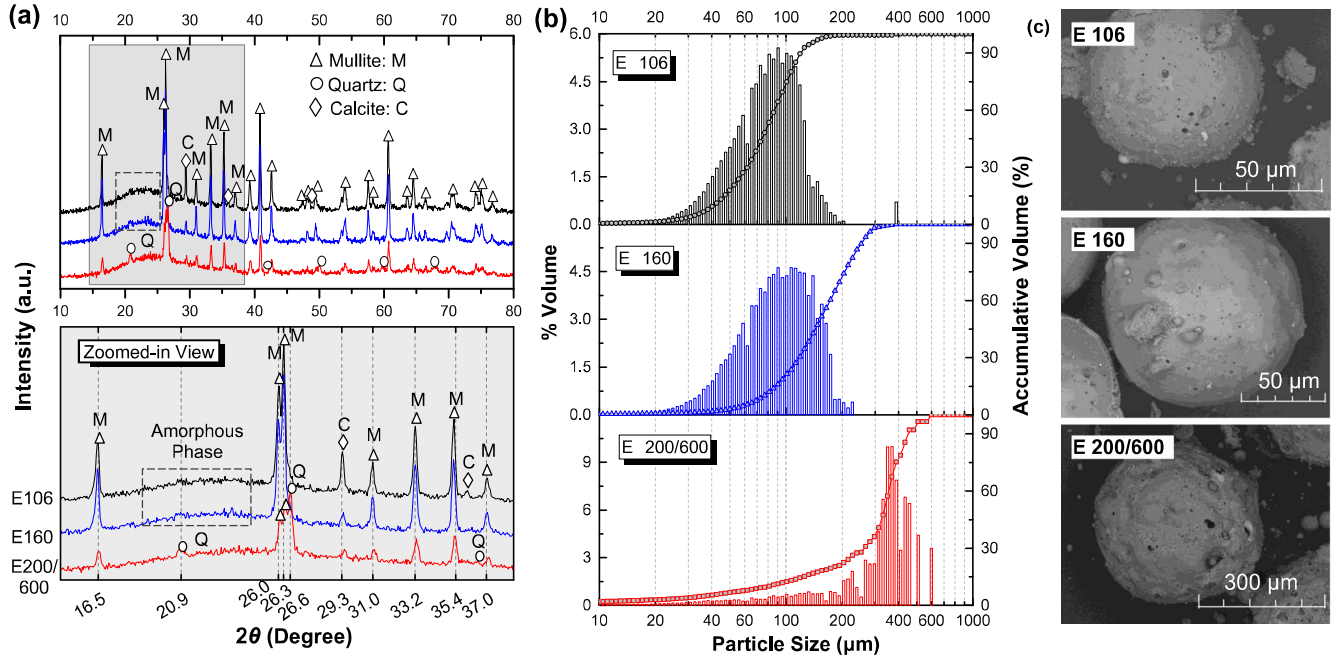

Fig. 1. Characterization of fly ash cenospheres (FAC): (a) XRD-analysis result and phase chart; (b) and particle size distribution of the fly-ash cenospheres (FAC), and (c) surface morphology of the FACs.

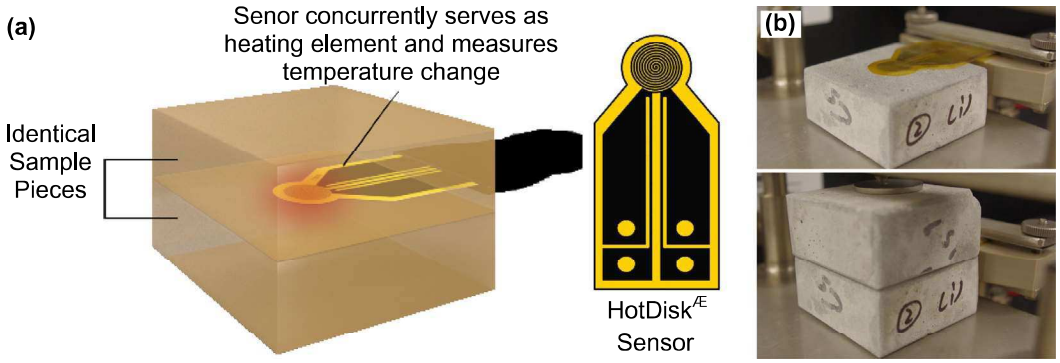

Fig. 2. The Transient Plane Source (TPS) tests for determining thermal properties: (a) illustrative of the test setup; (b) pictures showing the LWCC being tested.

2.3. Mechanical testing

Mechanical properties of the LWCC mortar mixtures were tested using a MTS-810 servo-hydraulic universal testing system. The loading was carried out in a displacement-control mode at the loading rate of 0.01 mm/min. Five 50 mm diameter by 100 mm tall cylinders were tested for each mixture group. A high resolution CCD camera was staged to record the damage and failure of the specimens. The mechanical test setup is shown in Fig. 3. The tested specimens were preserved for further morphological analysis.

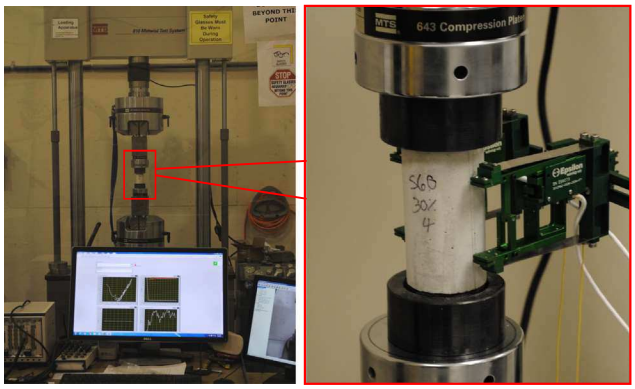

Fig. 3. Picture showing the mechanical test setup.

3. Results and discussions

3.1. Thermal and mechanical properties

3.1.1. Thermal test results

The experimental test results for density, thermal and mechanical properties of the lightweight cementitious composites (LWCC) are summarized in Table 2. The density of LWCC mortar samples was determined under both wet and oven-dry conditions. The wet density of mortar mixes was measured immediately after the cylinders were made. The oven dry density of LWCC was measured after 28 days curing and the samples were dried in a convection oven at 110 °C for 48 h. The oven dry density of the LWCC

Table 2
Density, mechanical, and thermal properties of the tested mixture groups.

Mix ID	LWMI material type	LWF fraction v_f (%)*	Air content (%)**	Wet density (kg/m^3)	Oven dry density (kg/m^3)	Compressive strength (MPa)	Thermal conductivity (W m^{-1} K^{-1})	Volumetric heat capacity (kJ/m^3)***
EPS-M-0	EPS beads (2.5 mm)	0	4.25	2351.61	2044.15	39.31	2.45	1505.2
EPS-M-1		6.75	–	2194.09	1911.09	36.51	1.96	1525.2
EPS-M-2		13.75	–	2041.36	1769.32	28.91	1.54	1340.7
EPS-M-3		21.00	–	1847.74	1612.15	20.32	1.15	1175
EPS-M-4		28.50	–	1498.13	1310.72	12.47	0.86	1013.6
EPS-S-0	EPS beads (1mm)	0	3.75	2343.11	2084.49	43.59	2.50	1472.4
EPS-S-1		6.75	–	2131.78	1885.19	36.29	1.87	1498.3
EPS-S-2		13.75	–	1922.17	1704.75	26.09	1.42	144369
EPS-S-3		21.00	–	1697.49	1502.72	18.67	1.03	1308.0
EPS-S-4		28.50	–	1486.55	1300.15	12.73	0.71	1146.2
TPMS-0	Thermoplastic microsphere	0	4.25	2260.74	2006.28	49.71	2.23	834.1
TPMS-1	(Expancel™)	6.75	–	2142.79	1846.30	40.52	1.70	1525.1
TPMS-2		13.75	–	1995.89	1731.07	32.35	1.31	1477.3
TPMS-3		21.00	–	1960.71	1646.53	25.68	1.07	1394.2
TPMS-4		28.50	–	1609.34	1372.05	12.68	0.69	689.5
K25-0	Hollow glass microsphere (3M)	0	5	2277.64	1974.11	55.10	2.30	1523.4
K25-1	K25	7.1	3	2235.54	1926.16	57.50	1.90	1595.2
K25-2		14.5	2	1984.32	1737.42	46.36	1.33	1358.2
K25-3		22.1	2.5	1737.39	1537.40	30.86	0.90	1222.1
K25-4		29.3	3.5	1588.65	1344.25	21.46	0.62	1207.3
S32-0	Hollow glass microsphere (3M)	0	4.5	2311.05	2013.08	51.33	2.19	1489.3
S32-1	S32	6.87	2	2238.87	1941.67	51.98	1.81	1564.0
S32-2		13.92	2.25	2067.02	1818.62	46.91	1.35	1547.5
S32-3		21.51	1.75	1901.02	1673.73	44.80	0.99	1274.8
S32-4		28.82	2	1664.36	1442.62	35.09	0.64	1194.9
S38HS-0	Hollow glass microsphere (3M)	0	3.25	2297.85	2026.87	45.99	2.18	1614.8
S38HS-1	S38HS	6.71	2.25	2218.99	1939.33	46.91	1.69	1628.6
S38HS-2		13.69	2	2058.28	1829.67	52.69	1.36	1599.3
S38HS-3		21.30	1	1871.48	1670.00	48.35	0.98	1311.7
S38HS-4		28.59	1.25	1654.59	1433.95	35.23	0.66	1220.7
H50-0	Hollow glass microsphere (3M)	0	4.25	2299.56	1989.22	50.07	2.26	1571.1
H50-1	H50	5.61	2.25	2173.20	1892.79	55.02	1.62	1595.7
H50-2		11.65	1.75	2127.71	1840.53	59.14	1.41	1545.8
H50-3		18.14	2	1943.72	1709.03	57.50	1.09	1451.2
H50-4		24.73	2	1773.87	1521.09	50.94	0.80	1369.3
S60-0	Hollow glass microsphere (3M)	0	4.75	2297.53	2006.69	48.72	2.15	1508.6
S60-1	S60	7.07	3.25	2208.98	1932.18	55.48	1.79	1625.8
S60-2		14.60	1.25	2088.87	1836.35	61.18	1.35	1581.2
S60-3		22.09	2.5	1903.32	1651.29	52.24	0.96	1439.4
S60-4		29.20	3.75	1697.20	1493.66	48.50	0.70	1272.8
E106-0	Fly-ash cenosphere E106	0	3.75	2288.17	1983.71	50.59	2.18	1638.0
E106-1		6.75	2.25	2178.57	1892.50	54.47	1.77	1597.9
E106-2		13.75	2.75	2054.27	1787.17	59.74	1.44	1557.9
E106-3		21.00	2.75	1910.69	1668.56	62.75	1.15	1460.4
E106-4		28.50	4.25	1705.88	1462.83	45.78	0.85	1321.7
E160-0	Fly-ash cenosphere E160	0	3.75	2296.20	2003.09	46.53	2.23	1648.4
E160-1		6.61	2.25	2145.89	1862.21	40.02	1.77	1444.2
E160-2		13.28	2.75	2039.50	1776.83	50.17	1.39	1519.9
E160-3		20.62	2.75	1870.99	1629.28	51.06	1.09	1420.9
E160-4		27.18	4.25	1656.77	1427.42	37.90	0.81	1188.9
E200/600-0	Fly-ash cenosphere E200/600	0	3.5	2333.19	2019.02	53.50	2.21	1590.0
E200/600-1		5.77	4.75	2160.37	1857.67	42.88	1.77	1585.4
E200/600-2		11.81	4.25	1991.62	1708.45	43.86	1.39	1486.9
E200/600-3		18.21	5.75	1840.96	1552.83	40.36	1.07	1354.3
E200/600-4		24.51	6	1654.94	1396.15	35.40	0.80	1387.9

* The LWF volume fraction is calculated as the ratio between the volume occupied by LWF over the total volume.
** The air content is measured on fresh LWCC mortars according to the ASTM 185–15c specifications.
*** The specific heat capacity is calculated based on the thermal diffusivity measured through the TPS method.

mixtures in this research ranges from 1300 kg/m^3 to 1940 kg/m^3 depending on the volume fraction and type of lightweight micro-filler aggregates used. The highest LWF volume fraction tested was about 28% with realistic consideration of the material costs.

In general, the thermal conductivity of LWCC mortar decreases with the increase in LWF volume fraction v_f. For the control mortar samples (without LWF), the thermal conductivity was tested between 2.1 and 2.2 W/m K. The thermal conductivities of LWCCs are significantly lower than that of normal weight cement mortar and concrete due to the incorporation of hollow (or porous) light-weight particulate fillers. It should be mentioned that since the LWFs were used to replace the regular fine aggregate (i.e., silica sand) by its equivalent volume. The decrease in thermal conductivity is partially attributed to two factors: (1) the inclusion of low

conductivity LWFs in cement paste, and (2) the decreased volume fraction of silica sand (i.e., silica sand, which is primarily quartz, has substantially higher thermal conductivity than cement paste. The thermal conductivity of cement paste at w/c = 0.43 was tested at 0.662 ± 0.0081 W/m K by transient plane source (TPS) method.) The contributions from sand and the LWF to the overall thermal conductivity of the LWCC composite mortar will be quantitatively discussed in later sections of this paper.

It was observed that the thermal conductivity of LWCC is relatively insensitive to the type and size of LWF used; rather, it is primarily dictated by the LWF volume fraction, see Fig. 4(a)–(c). As the LWF volume fraction v_f increases the equivalent thermal conductivity of LWCC mortar decreases notably, i.e., whenv_f = 7%, the thermal conductivity reduces by about 30%; as v_f approaches 28%, the thermal conductivity of LWCC decreases to 0.65–0.8 W/m K only 35% of the control mortar group. For the LWF materials studied herein – i.e., EPS beads/ETM, HGMs, and FAC, the particle size and shell property have very limited effects on the thermal conductivity of LWCC mortar. While LWCC containing larger particles (i.e., EPS-M, GHM K25, and FAC E200/600) has shown slightly higher thermal conductivity than other groups, see Fig. 4(a)–(c). This is mainly due to the greater air cell size induced within the mortar system by the larger size particles – i.e., the convective heat transfer through air enclosed in the cells reduces as the pore size becomes smaller [34]. Through the TPS method, the volumetric heat capacity of LWCCs can also be calculated from the thermal conductivity and thermal diffusivity tested. Generally, the volumetric heat capacity (VHC) of LWCC decreases as v_f increases and it ranges from 690 kJ/m^{3}K to 1680 kJ/m^3. The VHC is roughly proportional to the materials' dry density, see Fig. 4(d).

3.1.2. Compressive strength

Unlike thermal properties, the compressive strength of the LWCC depends largely on the type and size of LWF included. The average 28-day compressive strength of LWCC mixtures with different lightweight functional fillers and volume fractions (v_f) are summarized in Fig. 5, where the compressive strength is plotted against dry density of the materials. For LWCCs with EPS beads and expandable thermoplastic microspheres (ETM), the compressive strength decreases quickly as v_f becomes higher, see Fig. 5(a). The decrease in strength is primarily due to the introduction of the weak aggregate phase which promotes stress cracks to initiate and propagate within the materials under mechanical loading. While previous studies by Roy et al. on EPS concrete [35] indicated that smaller particle size normally yields higher strength, the difference in compressive strength between two different size EPS mortar groups (i.e., 2.5 mm and 1 mm) is not noticeable, see Fig. 5(a). However, it was observed that when v_f is small the compressive strengths of LWCC mixtures with ETM are about 15% higher than those of their EPS counterpart. This is believed to be caused by the reduction of air content due to the inclusion of ETM particles.

The compressive strength of LWCC mortars containing HGM and FAC, on the other hand, depends highly on the particle size and shell property (e.g., thickness) of the LWF included. When v_f is small (<15%), the compressive strength of LWCC mortars

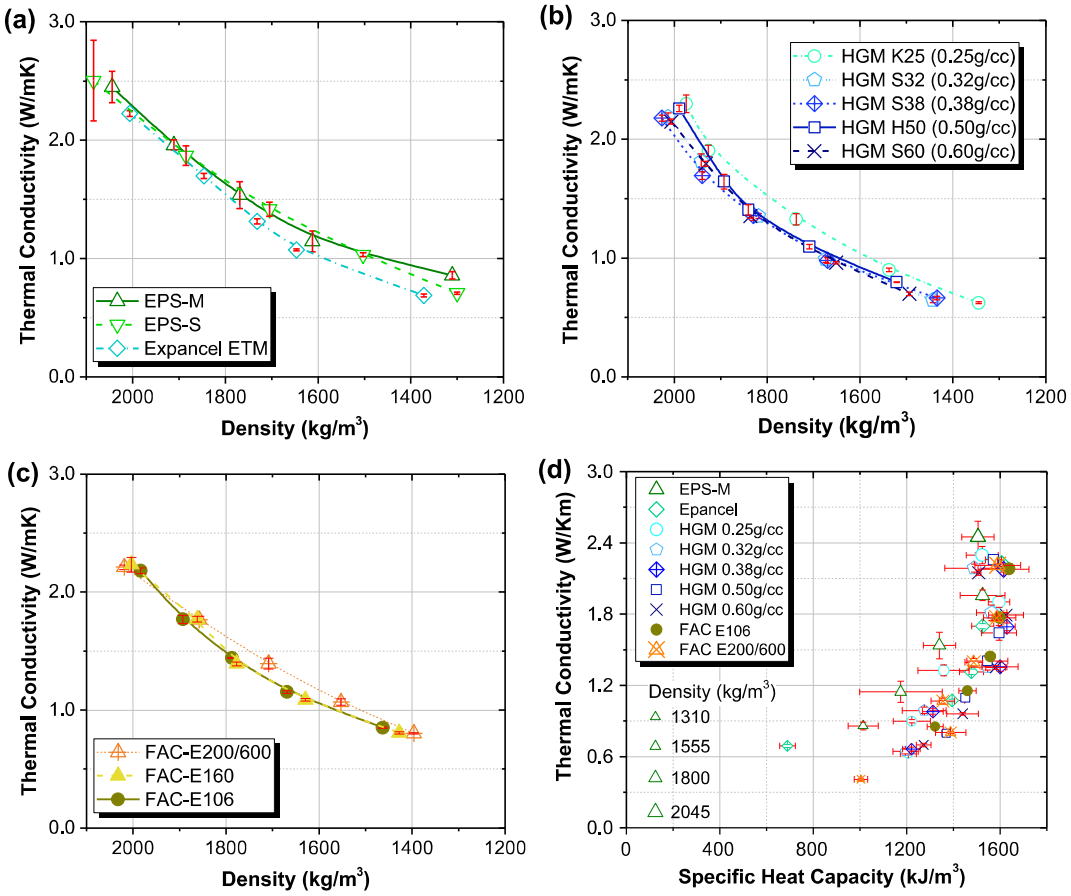

Fig. 4. Thermal properties of LWCC tested through Transient Plane Source (TPS) method: (a) LWCC with EPS beads and expandable thermoplastic microspheres (ETM); (b) LWCC with hollow glass microspheres (HGM); (c) LWCC with fly ash cenospheres (FAC); and (d) thermal conductivity vs. volumetric specific heat capacity tested through TPS.

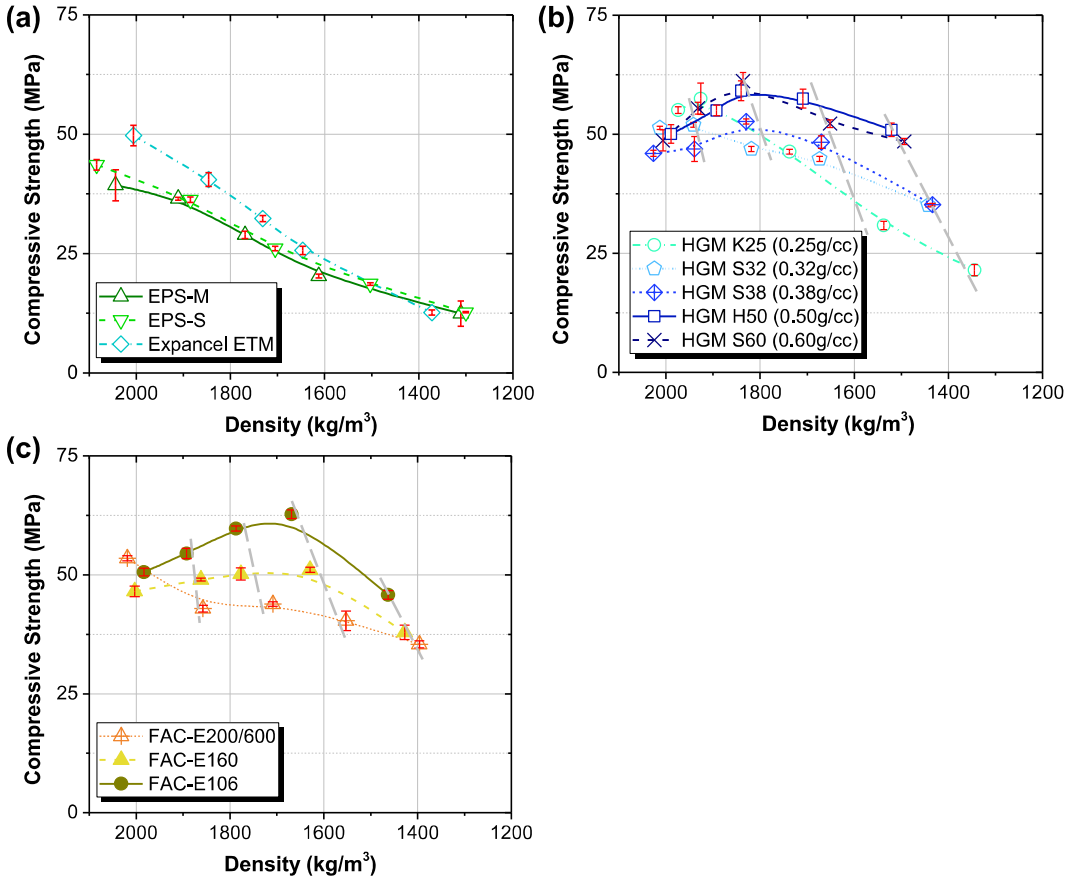

Fig. 5. Compressive strength vs. dry density of LWCCs containing: (a) EPS beads and ETM; (b) hollow glass microspheres (HGM); and (c) fly-ash cenospheres (FAC).

increases with higher HGM concentrations, see Fig. 5(b). This is believed to be due to the spherical shape of HGM, which improves the rheological property (i.e., flowability) of fresh mortar mixes and reduces the air content (Table 2). The compressive strength starts to decrease when the volume fraction of HGM becomes higher (>15%) – i.e., the hollow structure of HGMs allows the stress cracks to propagate through the particle shell to cause damage and material failure. It is noted that with the same LWF volume concentration (or density), mortars having smaller size HGM particles and thicker shell yield higher mechanical strength, see Fig. 5(b). This trend becomes more notable when LWF volume fraction v_f is high. At v_f = 7%, the HGM S60 mortar is 32% (15 MPa) stronger than the mortar containing K25 particles; whereas at v_f = 28%, S60 mortar is about 125% (27 MPa) stronger than the K25 mortar. It is worthwhile mentioning that the compressive strength of LWCC mortars mixed with nearly 30% (total volume fraction) of H50 and S60 HGM particles are almost the same as the reference mortar while their densities were about 25% lower than the reference mortar, see Table 2 and Fig. 5(b). This provides significant potential for the design of high strength lightweight cementitious composites and concretes for structural applications.

A similar trend was observed for LWCCs containing FACs. Generally, LWCC containing larger FAC particles (i.e., E200/600) have lower strength for given FAC volume fraction (or density). For the LWCC group having E200/600 cenospheres, the compressive strength shows a continuously descending trend as v_f becomes higher. For both E106 and E160, the mortar strength peaks at v_f = 21% and it decreases rapidly (by about 25%) when v_f approaches 28%. For LWCCs modified with E106 and E160 FAC, the compressive strength is similar or higher than the reference mortar when the v_f is less than 20–25%, see Fig. 5(c). It is noted that the E200/600 mortars have higher air content than the other FAC groups (Table 2). This is likely due to the surface pores on the cenospheres (Fig. 1(c)) as well as the larger particles size that made the fresh mortar less flowable.

3.2. Microstructures and fracture topography

The microstructural characterization was carried out using scanning electron microscopic (SEM) imaging. The LWCC mortar samples for microstructural analysis were resin-impregnated using epoxy, and the resin mounted samples were then ground and polished using a Buehler EcoMet grinder/polisher to 0.3 μm diamond paste. Some polished samples were then carbon-coated to a thickness of approximately 10 nm to prevent charging under the electron beam. SEM imaging was conducted using a Hitachi TM1000 at accelerating voltage of 15 kV. For analyzing the fracture surfaces of LWCC, fragments of the tested compression cylinders were preserved and placed on a sample holder for SEM imaging analysis.

Fig. 6 presents the SEM micrographs of four different LWCCs having E 200/600, E160 FACs and K25, S60 HGMs as the lightweight filler. The volume fractions of LWF for the four LWCC groups presented in Fig. 6 were nearly the same, i.e., approximately 14% of the total volume. It is noted that the E200/600 FAC have similar particle size with silica sand and the cenospheres were scattered across the mortar material (Fig. 6(a)). The shell thickness of E200/600 FAC is around 15 μm (5–10% of the particle diameter) and the shell has a microporous structure. On the other hand, the smaller FAC particles (E160) are well distributed within the cementitious binder, see Fig. 6(b). The denser, more compacted,

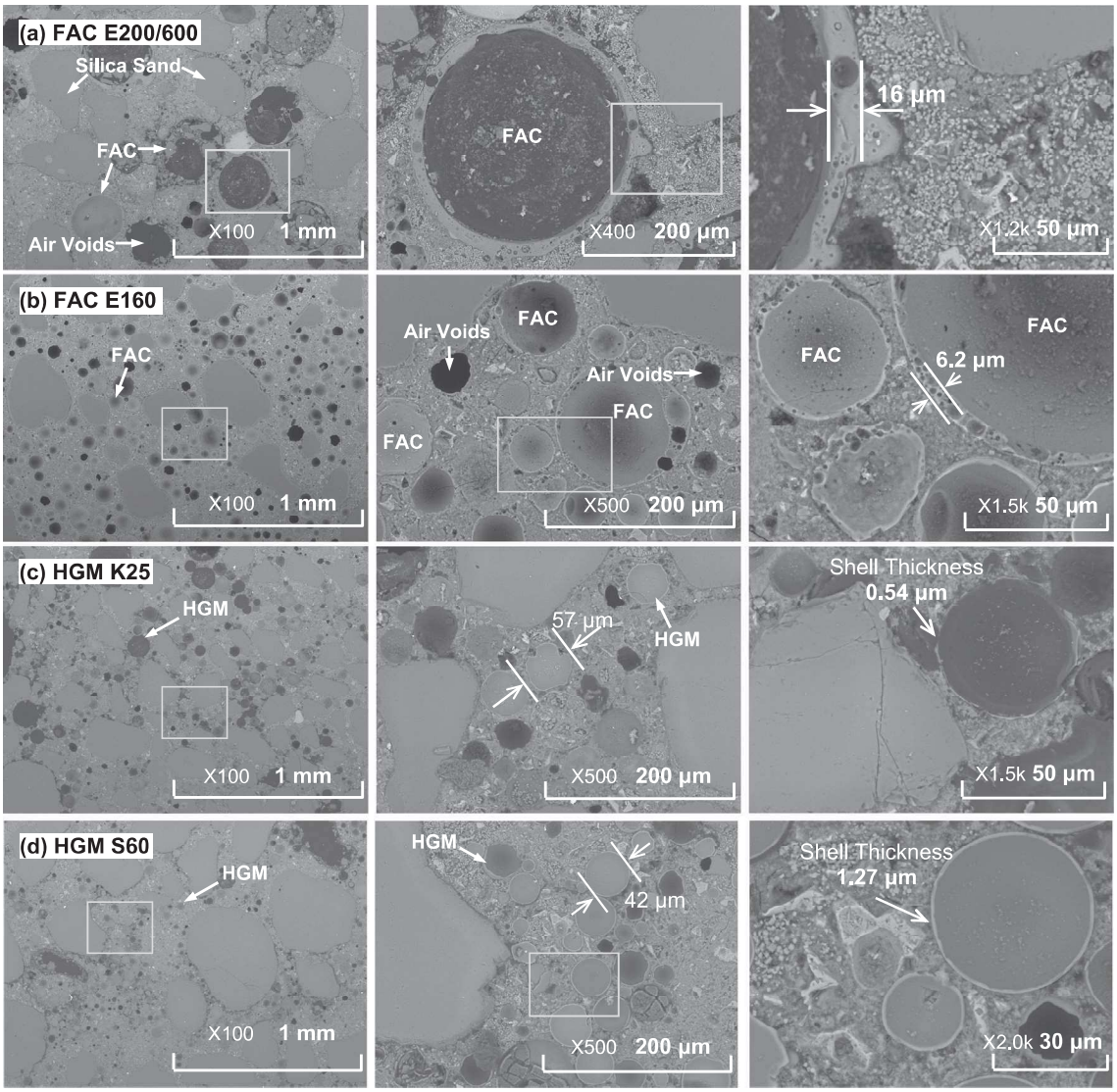

Fig. 6. SEM images showing the microstructure of LWCC containing (a) E200/600 fly ash cenosphere (FAC); (b) E160 FAC; (c) K25 HGM (0.25 g/cm^3); and (d) S60 HGM (0.60 g/cm^3).

and uniform microstructure in the E160 modified LWCC influenced its mechanical strength (Fig. 5(c)) and other properties of the composites including the post-crack behavior [36]. It was also observed in the experiments that the spherical shape and smooth surface of E106 and E160 FAC (see Fig. 1(c)) improved the rheological behavior of the fresh mortar mix and reduced the air content. The K25 and S60 HGMs have similar particle size as the E160 FAC and they were both well distributed within the cementitious binder. While the low density K25 particles have greater particle size and thinner shell wall than S60 (see Table 1 and Fig. 6 (c) and (d)), it is evident that most of the K25 and S60 HGM particles survived the mortar mixing process and breakage of LWF particles during concrete mixing are minimal.

The fracture surfaces of the compressive cylinders used for the mechanical testing were also examined using SEM. Fig. 7 presents the fracture topographical images of six different LWCC mixtures including EPS-small, expandable thermoplastic microsphere (ETM), FAC200/600, FAC160, HGM K25 and HGM K60. It is evident that the damage modes of materials at microscopic scale are different for the various LWF types used in this research. For LWCC containing EPS beads, the lightweight aggregates mostly act as weak points within the mortar system which promote the initiation and percolation of stress cracks, see Fig. 7(a). Similarly, the ETM particles within the LWCC are too weak to resist the microcracks developed within the material even though its particle size is much smaller than that of EPS, see Fig. 7(b). Therefore, as the LWF volume fraction v_f increases, the strengths of both EPS and ETM groups decrease continuously, see Fig. 5(a), even though the LWCC containing ETM has shown marginally higher strength when v_f is low. This is believed due to the lubrication effect of ETM particles which reduced the air content of the mortar.

The fracture surface of HGM K25 modified LWCC have shown a large amount of particle breakage inside the tested mortar. The low shell thickness to particle size ratio (t/D) leads to its relatively low crush strength (Table 1). The low mechanical strength of these particles could not resist the stresses within the LWCC composites [36] and the stress cracks mostly propagated through the K25 HGM particles, see Fig. 7(c). On the other hand, the LWCCs incorporating HGM S60 particles showed a different behavior. The S60 particles are generally smaller in size (with average particle size around 30 µm) and have thicker shell (about 1.5 µm in thickness) as compared to the K25 particles. As a result,

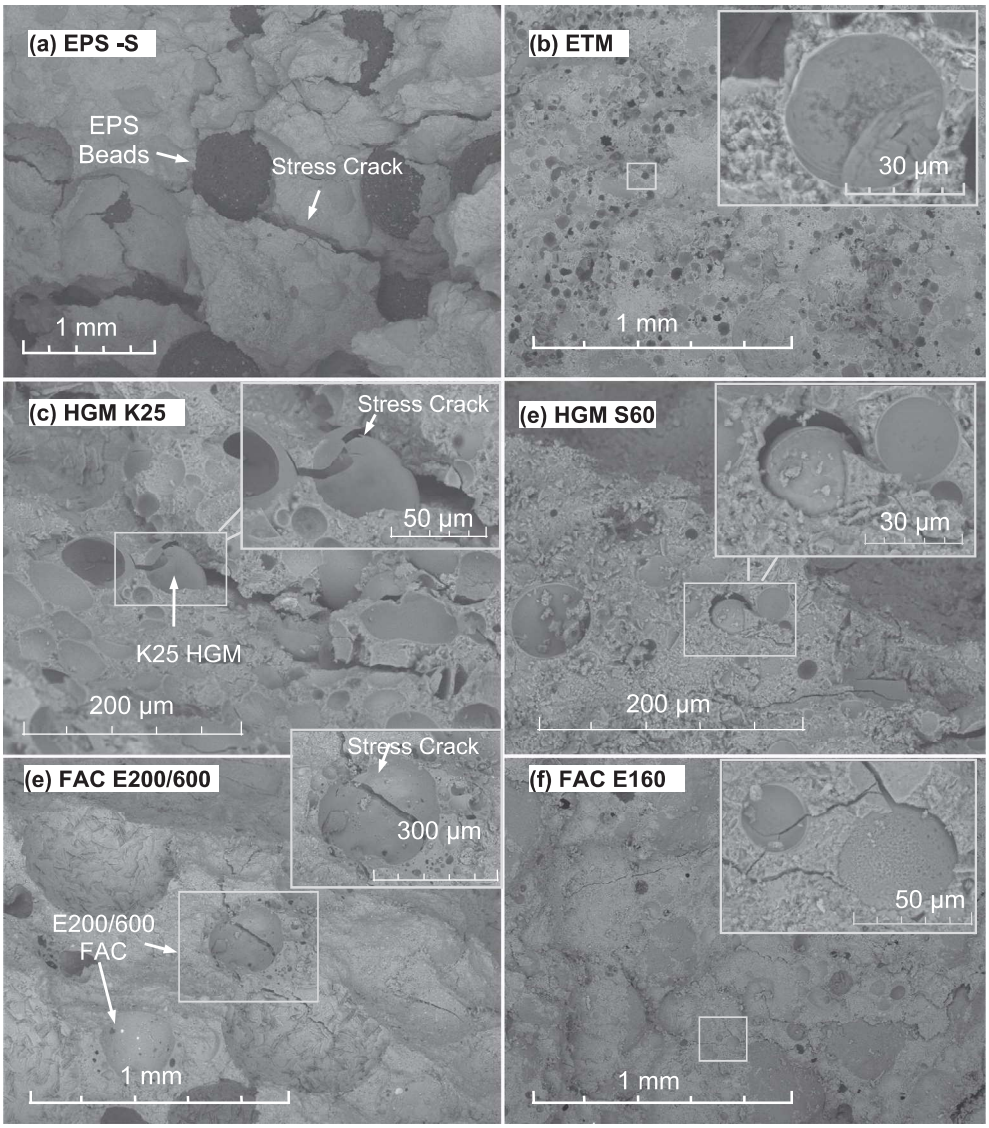

Fig. 7. Fracture topography showing the fracture surfaces of LWCCs containing: (a) EPS beads (1 mm); (b) ETM plastic microsphere; (c) K25 and (d) S60 glass microspheres; and (e) E200/600 and (f) E160 FAC.

the S60 HGM has much higher isostatic crush strength as noted in Table 1. The higher mechanical strength of LWF particles would alter the damage mode within the LWCC material, where it can be observed that the crack growth was resisted by the HGM S60 particles by hindering its path. While some S60 particles did break, many particles within the mortar have shown pull-out instead of shell breakage, see Fig. 7(d). Moreover, weak ITZ (interfacial transition zone) characteristics and debonding were also observed for HGM particles.

The LWCC containing fly ash cenospheres (FAC) generally exhibit good mechanical performance, see Fig. 5(c). For all three types of FACs studied in this research, the FAC particles bonded well with the cementitious matrix, owing to the micro-porous surface of FACs (Fig. 1(c)) as well as its partial pozzolanic reactivity [37]. It was revealed in the XRD analysis (Fig. 1(a)) that FAC particles contain amorphous silica which can react with the pore solution (i.e., calcium hydroxide) in the reacted cementitious binder. Similar to HGM, the larger FAC particles (E200/600) allow stress cracks to propagate through their shell (Fig. 7(e)) whereas the smaller E160 FAC may act as barriers to hinder the propagation of stress cracks (Fig. 7(f)).

3.3. Thermal conductivity of LWCC containing particulate LWFs

The effective thermal conductivity of lightweight cementitious composites (LWCC) containing hollow sphere particles can be calculated based on the equations proposed by Felske [38] as a function of the properties of each composing phase, their volume fractions, and the contact thermal resistance at the particle-to-matrix interface:

$$k_{eff} = k_1 \frac{2(1-v_f)\Omega + \Gamma_N \beta}{(2+v_f)\Omega + \Gamma_D \beta} \tag{2}$$

where

$$\Omega = (2+v_{f3})\frac{k_3}{k_2} - 2(1-v_{f3}) \tag{3}$$

and

$$\Gamma_N = (1-v_f)\left[2(1+2v_{f3}) - 2\frac{k_3}{k_2}(1-v_{f3})\right] + (1+2v_f)\left[\frac{k_3}{k_1}(2+v_{f3}) - 2\frac{k_2}{k_1}(1-v_{f3})\right] \tag{4}$$

$$\Gamma_D = (2+v_f)\left[(1+2v_{f3}) - \frac{k_3}{k_2}(1-v_{f3})\right] + (1-v_f)\left[\frac{k_3}{k_1}(2+v_{f3}) - 2\frac{k_2}{k_1}(1-v_{f3})\right] \quad (5)$$

where v_f is the volume fraction of the LWF particles; k_1 is the thermal conductivity of the cement paste; k_2 is the thermal conductivity of the LWF shell; v_3 and k_3 are the volume fraction and thermal conductivity of the cavity (air), respectively; and β is the interfacial thermal resistance, see Fig. 8(a). Note that:

$$v_{f3} = \frac{v_f}{v_3} = \left(\frac{r_2}{r_3}\right)^3 \quad (6)$$

and the density of the LWF particle, u, is:

$$u = \left(1 - \frac{r_3^3}{r_2^3}\right)\rho_s \quad (7)$$

where ρ_s is the shell density of the hollow spheres, and the mass of air in the cavity is neglected. From Eqs. (6) and (7) we simply have:

$$v_{f3} = \frac{\rho_s}{\rho_s - u} \quad (8)$$

Thus, the effective thermal conductivity of LWCC filled with spherical LWFs, i.e., Fig. 8(b), can be expressed in terms of the particle volume fraction, v_f, the thermal conductivities of each included phase, and the measured density of the LWF particle, u. Note that the density of LWF particles can be experimentally measured by methods including gas pycnometry [39] and is often reported in the particle manufacturer data sheets.

Since the thermal conductivity of air is notably lower than the other two solid phases – i.e., the cement paste and microsphere shell ($k_3 \to 0$) and assuming perfect thermal contact between the cement matrix and LWF ($\beta \to \infty$), then substituting Eq. (8) into Eq. (2) we have:

$$k_{eff} = \left[\frac{(\eta+2)+2(\eta-1)v_f}{(\eta+2)-(\eta-1)v_f}\right]k_1 \quad (9)$$

where $\eta = 2k_{21}u/(3\rho_s - u)$, and $k_{21} = k_2/k_1$. Thus, the effective thermal conductivity of LWF filled cement paste can be simply calculated as a function of the thermal conductivity of the cement paste matrix, k_1, particle volume fraction, v_f, density, u, and the LWF shell properties, k_2 and ρ_s. It is worthwhile noting that for Eq. (2) or Eq. (9), the thermal conductivity of micro-size LWF particles, which is proved to be difficult to experimentally obtain [19], is not required for calculating the equivalent thermal property.

It is noted that for LWF modified by phase changing materials (PCMs) [40], Eq. (9) can be modified to account for the thermal conductivity and the temperature-dependent heat capacity of PCMs [41].

For LWCCs with fine aggregates (e.g., silica sand, Fig. 8(c)), the homogenized effective conductivity and specific heat capacity can then be calculated by treating the LWF filled cement paste as a homogenized matrix phase with regular fine aggregates dispersed in it (a two phase composite system as shown in Fig. 8(c)). Thus, many two-phase homogenization methods such as the Maxwell-Garnett model [40], Hashin and Shtrikman model [41] and generalized self-consistent method [42–44] can be used to calculate the equivalent thermal properties.

Fig. 9 shows the comparison between the calculated thermal conductivities of HGM (i.e., K25, S32, H50, and S60) filled cement mortars versus the values measured by the TPS method. At w/c = 0.43, the thermal conductivity of cement paste matrix (k_1) was tested at 0.66 W/mK. The LWF particle properties involved in Eq. (9) – i.e., particle density, u, are listed in Table 2; the shell density, ρ_s, of TPMS, HGM, and FAC are 0.975 g/cm^3, 2.51 g/cm^3, and 2.03 g/cm^3, respectively; and thermal conductivity of shell material, k_2 for TPMS, HGM, and FAC are 0.15 W/mK, 1.05 W/mK, and 0.62 W/mK, respectively. The specific density and thermal conductivity of silica sand were taken as 2650 kg/m^3 and 7.5 W/mK. Since the decrease in thermal conductivity is partially due to the reduction of sand ratio, the thermal conductivities of cement mortars having the same sand to binder ratio (without LWMF) corresponding to each LWMF volume concentration are plotted in Fig. 9 for the purpose of comparison. The experimental data and the predicted results for mortar samples with four types of HGMs are compared. It shows a close match between experimental tested data and the predicted results. Since the thermal conductivity is shown to be insensitive to the type of LWF by both the experimental results (Fig. 4) and the Felske model predictions, the comparisons for all 55 mixture groups are not redundantly shown herein.

3.4. Thermal conductivity and strength: The implication on building structural and energy performance

Fig. 10 presents the mechanical and thermophysical property map tested for the LWCCs, where the material's thermal conductivity is plotted against the compressive strength and the color contour indicates dry density. Unlike the correlations between thermal and mechanical properties of traditional lightweight aggregate concrete [2], foamed cellulous concrete [45], and EPS concrete [22] where the strength is inversely proportional to the material's thermal resistance, the thermal-mechanical property map of LWCC containing micro-size LWF fillers has shown large design space. The material properties can be fine-tuned by varying the volume fraction, size, and shell property of LWF. Since the thermal conductivity and specific heat capacity are primarily functions of the LWF volume fraction, the dependency of the material's mechanical performance on the size and shell property of LWF provides opportunities to develop high performance structural

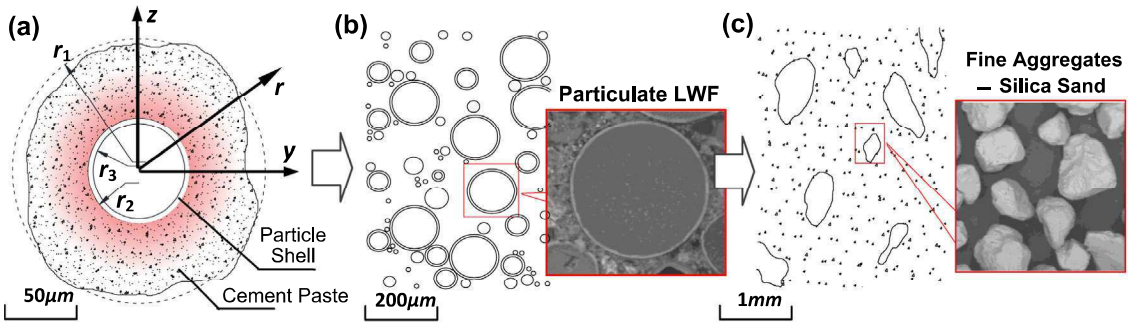

Fig. 8. Microstructure and effective thermal conductivity of lightweight cementitious composite (LWCC): (a) a RVE containing one single microsphere particle; (b) cement paste with polydispersed microsphere particles; and (c) LWCC mortar with fine aggregates (e.g., silica sand).

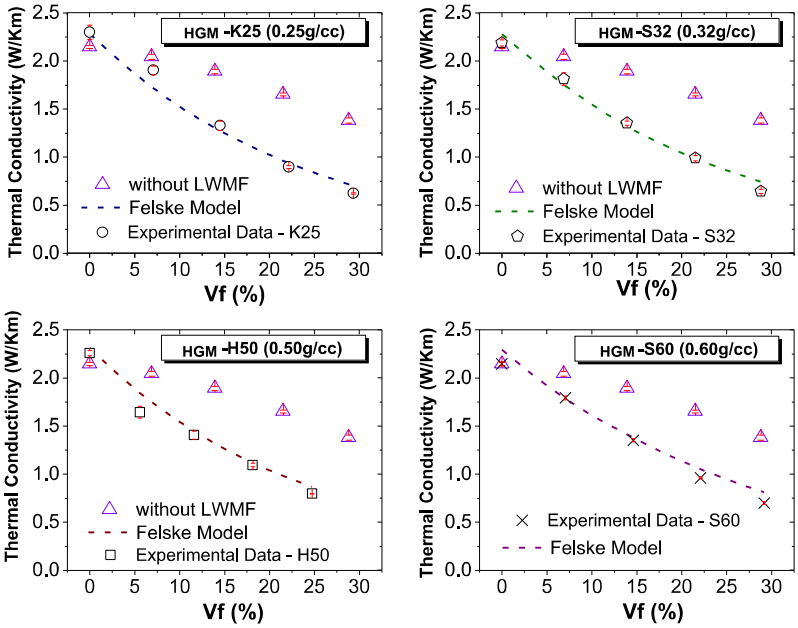

Fig. 9. Comparisons between the predicted thermal conductivities as functions of the LWF volume fraction.

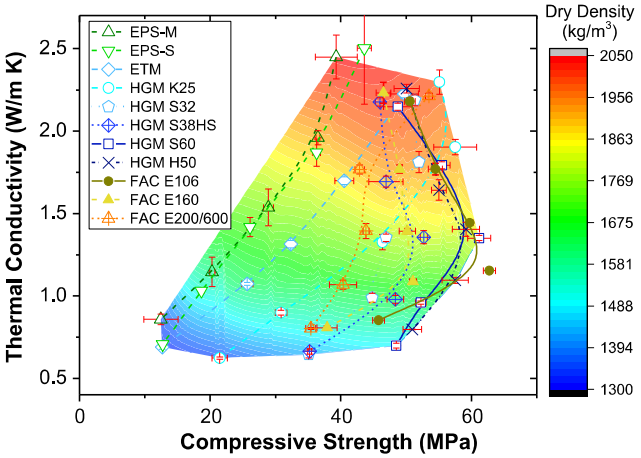

Fig. 10. Thermal and mechanical properties map of LWCC.

materials that have high mechanical strength whilst possessing the desired thermophysical properties such as lightweight, low thermal conductivity, and even latent heat storage (e.g., the study on PCM loaded cenospheres by Liu et al. [40]). Fig. 11 presents the correlations of strength and thermal resistance of four different LWCCs tested in this study as functions of the LWF volume fraction (i.e., R-value is calculated for a 15 cm wall made from such material). It can be seen that high strength and high insulation building/structural material can be produced by incorporating smaller size LWF particles with strong shells.

4. Conclusions

A comprehensive study on lightweight cementitious composites (LWCC) incorporating various types of lightweight filler (LWF) materials, including expanded polystyrene (EPS) beads, expandable thermoplastic microsphere (ETM), hollow glass microspheres (HGM), and fly ash cenospheres (FAC), was conducted to evaluate the influence of LWFs and their corresponding particle properties (i.e., size, volume fraction, and shell thickness etc.) on both the mechanical and thermophysical properties of LWCC. The microstructural properties were analyzed for both pristine and mechanically tested samples. Key parameters governing thermal and mechanical properties of the material are discussed, and the composition-property relationships are deduced from both experiment results and predictive models. The following conclusions are drawn from this study:

- The mechanical and thermal properties of lightweight cementitious composites, or LWCC, are greatly affected by the type and properties of the lightweight functional filler (LWF) used. To achieve the desired lightweight feature while still maintaining adequate mechanical properties, careful selection and efficient utilization of LWF materials is imperative.
- The thermal properties (i.e., thermal conductivity and specific heat capacity) of LWCCs are primarily dictated by the volume fraction of LWF and they are insensitive to the type of LWF used; on the other hand, the mechanical properties of LWCC are greatly affected by the LWF particle properties including the size, shell thickness (stiffness), and interfacial bonding between the particles and cementitious binder.
- Because of the high strength-to-unit weight ratio, most fly ash cenospheres (FAC) and hollow glass microspheres (HGM) with higher density (e.g., H50 and S60) are suitable for producing lightweight cementitious composite (LWCC) materials that may be used for structural load bearing, as long as the LWF volume fraction is controlled within a reasonable range. It is noted that even though the compressive strength of LWCC may be satisfactory for structural purposes, their Young's moduli are normally lower than those of normal weight concrete. In addition, cautions should be taken when using large size FACs in the LWCC mixtures (e.g., E200/600 studied in this research), as their large particle size (i.e., >500 μm) may change the rheological property of the fresh mortar mix and cause workability issues.
- Generally, LWFs with soft polymeric shells, including EPS beads and dry-expanded thermoplastic microspheres (ETM), and HGM with lower density may be suitable for producing non

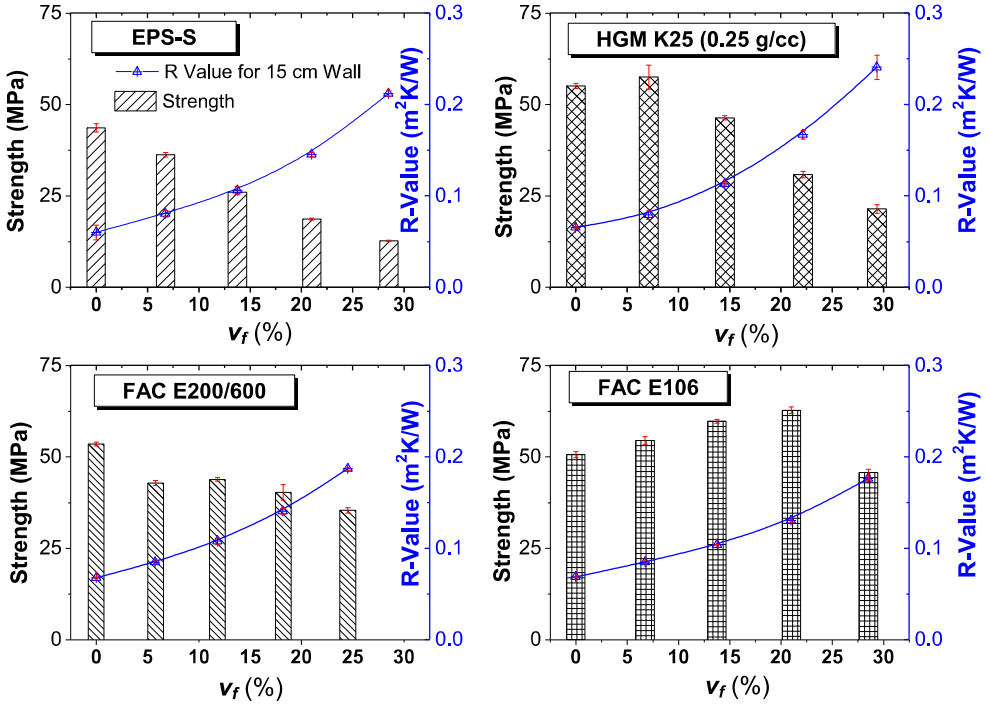

Fig. 11. Correlations between compressive strength, thermal resistance (R-value), and the volume fraction of LWF particles.

loadbearing members such as partition walls and ceiling panels, etc. However, mixing ETM at the construction site may be challenging (if at all feasible) due to its very low density. The ETM particles tend to become air-borne when stimulated by the mixer.

- SEM analysis performed on the mechanically tested LWCC samples revealed that most LWF particles with lower shell thickness-to-diameter ratio (t/D) broke within the composite when subjected to mechanical loading, while strong LWF particles with smaller particle size and thicker shell walls would survive the mechanical load and show "pull-out" failure within the LWCC composite.
- The Felske equation provides a simple yet accurate method to calculate the thermal property of LWCCs containing particulate LWF. The included LWF particles can have both core-shell (i.e., HGM and FAC) or porous (e.g., EPS) configurations, and they can be polydispersed within the cementitious matrix binder. The equations can also be used for calculating the thermal conductivity and specific heat of composites containing phase changing materials (PCMs) by simply replacing the air phase to PCM and considering the temperature-dependent heat capacity of PCM.
- Lastly, by carefully selecting the functional micro-size filler, LWCCs with high strength and low thermal conductivity can be developed to reduce the operational energy consumption over a buildings' use phase.

Acknowledgements

This research was partially sponsored by National Science Foundation (CMMI-1663302). The funding support from NSF and the University of Alabama in Huntsville is greatly appreciated. The authors would also like to thank the material donations from 3M (glass microsphere bubbles) and Expancel (thermoplastic microspheres), as well as the insightful discussions from Mr. Robert Hunter and Mr. Kevin Rink from 3M Advanced Materials Division.

References

[1] E. Yasar, C.D. Atis, A. Kilic, H. Gulsen, Strength properties of lightweight concrete made with basaltic pumice and fly ash, Mater. Lett. 57 (2003) 2267–2270, https://doi.org/10.1016/S0167-577X(03)00146-0.
[2] J.L. Clarke (Ed.), Structural Lightweight Aggregate Concrete, Blackie Academic & Professional, London and New York, 1993.
[3] International Energy Agency, Transition to Sustainable Buildings: Strategies and Opportunities to 2050, Paris, 2013. doi:10.1787/9789264202955-en.
[4] D. Kramar, V. Bindiganavile, Mechanical properties and size effects in lightweight mortars containing expanded perlite aggregate, Mater. Struct. 44 (2011) 735–748, https://doi.org/10.1617/s11527-010-9662-0.
[5] M. Lanzón, P.A. García-Ruiz, Lightweight cement mortars: advantages and inconveniences of expanded perlite and its influence on fresh and hardened state and durability, Constr. Build. Mater. 22 (2008) 1798–1806, https://doi.org/10.1016/j.conbuildmat.2007.05.006.
[6] Z. Lu, B. Xu, J. Zhang, Y. Zhu, G. Sun, Z. Li, Preparation and characterization of expanded perlite/paraffin composite as form-stable phase change material, Sol. Energy 108 (2014) 460–466, https://doi.org/10.1016/j.solener.2014.08.008.
[7] R. De Gennaro, A. Langella, M. D'Amore, M. Dondi, A. Colella, P. Cappelletti, et al., Use of zeolite-rich rocks and waste materials for the production of structural lightweight concretes, Appl. Clay Sci. 41 (2008) 61–72, https://doi.org/10.1016/j.clay.2007.09.008.
[8] Y. Ke, A.L. Beaucour, S. Ortola, H. Dumontet, R. Cabrillac, Influence of volume fraction and characteristics of lightweight aggregates on the mechanical properties of concrete, Constr. Build. Mater. 23 (2009) 2821–2828, https://doi.org/10.1016/j.conbuildmat.2009.02.038.
[9] A. Lotfy, K.M.A. Hossain, M. Lachemi, Lightweight self-consolidating concrete with expanded shale aggregates: modelling and optimization, Int. J. Concr. Struct. Mater. 9 (2015) 185–206, https://doi.org/10.1007/s40069-015-0096-5.
[10] S. Chandra, L. Berntsson, Lightweight Aggregate Concrete: Science, Technology, and Applications, Noyes Publications, New York, 2002.
[11] American Society for Testing and Materials, Standard Specification for Lightweight Aggregates for Structural Concrete, 2017, doi:10.1520/C0330.
[12] America Concrete Institute, Standard Practice for Selecting Proportions for Structural Lightweight Concrete (ACI 211. 2-98), 1998.
[13] M. Hassanpour, P. Shafigh, H. Bin, Lightweight aggregate concrete fiber reinforcement – a review, Constr. Build. Mater. 37 (2012) 452–461, https://doi.org/10.1016/j.conbuildmat.2012.07.071.
[14] H. Aglan, S. Shebl, M. Morsy, M. Calhoun, H. Harding, M. Ahmad, Strength and toughness improvement of cement binders using expandable thermoplastic microspheres, Constr. Build. Mater. 23 (2009) 2856–2861, https://doi.org/10.1016/j.conbuildmat.2009.02.031.
[15] T.S. Yun, Y.J. Jeong, T.S. Han, K.S. Youm, Evaluation of thermal conductivity for thermally insulated concretes, Energy Build. 61 (2013) 125–132, https://doi.org/10.1016/j.enbuild.2013.01.043.

[16] Q. Zhang, V.C. Li, Development of durable spray-applied fire-resistive engineered cementitious composites (SFR-ECC), Cem. Concr. Compos. 60 (2015) 10–16, https://doi.org/10.1016/j.cemconcomp.2015.03.012.
[17] D. Oreshkin, V. Semenov, T. Rozovskaya, Properties of light-weight extruded concrete with hollow glass microspheres, Proc. Eng. 153 (2016) 638–643, https://doi.org/10.1016/j.proeng.2016.08.214.
[18] X. Huang, R. Ranade, Q. Zhang, W. Ni, V.C. Li, Mechanical and thermal properties of green lightweight engineered cementitious composites, Constr. Build. Mater. 48 (2013) 954–960, https://doi.org/10.1016/j.conbuildmat.2013.07.104.
[19] Y. Wu, J.Y. Wang, P.J.M. Monteiro, M.H. Zhang, Development of ultra-lightweight cement composites with low thermal conductivity and high specific strength for energy efficient buildings, Constr. Build. Mater. 87 (2015) 100–112, https://doi.org/10.1016/j.conbuildmat.2015.04.004.
[20] B. Xu, H. Ma, C. Hu, S. Yang, Z. Li, Influence of curing regimes on mechanical properties of magnesium oxychloride cement-based composites, Constr. Build. Mater. 102 (2016) 613–619, https://doi.org/10.1016/j.conbuildmat.2015.10.205.
[21] A. Hanif, P. Parthasarathy, H. Ma, T. Fan, Z. Li, Properties improvement of fly ash cenosphere modified cement pastes using nano silica, Cem. Concr. Compos. 81 (2017) 35–48, https://doi.org/10.1016/j.cemconcomp.2017.04.008.
[22] A.A. Sayadi, J.V. Tapia, T.R. Neitzert, G.C. Clifton, Effects of expanded polystyrene (EPS) particles on fire resistance, thermal conductivity and compressive strength of foamed concrete, Constr. Build. Mater. 112 (2016) 716–724, https://doi.org/10.1016/j.conbuildmat.2016.02.218.
[23] R. Madandoust, M.M. Ranjbar, Mousavi S. Yasin, An investigation on the fresh properties of self-compacted lightweight concrete containing expanded polystyrene, Constr. Build. Mater. 25 (2011) 3721–3731, https://doi.org/10.1016/j.conbuildmat.2011.04.018.
[24] Y. Xu, L. Jiang, J. Xu, Y. Li, Mechanical properties of expanded polystyrene lightweight aggregate concrete and brick, Constr. Build. Mater. 27 (2012) 32–38, https://doi.org/10.1016/j.conbuildmat.2011.08.030.
[25] S.A. Mousavi, S.M. Zahrai, A. Bahrami-Rad, Quasi-static cyclic tests on super-lightweight EPS concrete shear walls, Eng. Struct. 65 (2014) 62–75, https://doi.org/10.1016/j.engstruct.2014.02.003.
[26] A.S. Bubnov, V.S. Khorev, I.A. Boyko, The effect of lightweight agents on the density of cement slurry applied during oil and gas well drilling, IOP Conf. Ser. Earth Environ. Sci., Manchester (2015), https://doi.org/10.1088/1755-1315/24/1/012008.
[27] T. Ichikawa, M. Miura, Modified model of alkali-silica reaction, Cem. Concr. Res. 37 (2007) 1291–1297, https://doi.org/10.1016/j.cemconres.2007.06.008.
[28] K.V. Joseph, F. Francis, J. Chacko, P. Das, G. Hebbar, FLY ash cenosphere waste formation in coal fired power plants and its applications a structural material – a review, Int. J. Eng. Res. Technol. 2 (2013) 18–21.
[29] AkzoNobel, Expancel® 461 DET 40 d25 datasheet, 2017.
[30] 3M, 3M Glass Bubbles K Series, S Series and iM Series, 2009.
[31] ISO22007-2:2008, Plastics – Determination of thermal conductivity and thermal diffusivity – Part 2: Transient plane source method, 2008.
[32] T. Log, S. Gustafsson, Transient Plane Source (TPS) technique for measuring thermal transport properties of building material, Fire Mater. 19 (1995) 43–49.
[33] ASTM C1363, Standard Test Method for Thermal Performance of Building Materials and Envelope Assemblies by Means of a Hot Box Apparatus, 2005, doi:10.1520/C1363-11.2.
[34] K. Kaviany, Principles of Heat Transfer in Porous Media (Mechanical Engineering Series), Springer, Berlin, 1995. doi:10.1016/j.applthermaleng.2011.11.001.
[35] R. Le Roy, E. Parant, C. Boulay, Taking into account the inclusions' size in lightweight concrete compressive strength prediction, Cem. Concr. Res. 35 (2005) 770–775, https://doi.org/10.1016/j.cemconres.2004.06.002.
[36] A. Hanif, Z. Lu, Y. Cheng, S. Diao, Z. Li, Effects of different lightweight functional fillers for use in cementitious composites, Int. J. Concr. Struct. Mater. 11 (2017) 99–113, https://doi.org/10.1007/s40069-016-0184-1.
[37] V. Rheinheimer, Y. Wu, T. Wu, K. Celik, J. Wang, L. De Lorenzis, et al., Multi-scale study of high-strength low-thermal-conductivity cement composites containing cenospheres, Cem. Concr. Compos. 80 (2017) 91–103, https://doi.org/10.1016/j.cemconcomp.2017.03.002.
[38] J.D. Felske, Effective thermal conductivity of composite spheres in a continuous medium with contact resistance, Int. J. Heat Mass Transfer 47 (2004) 3453–3461, https://doi.org/10.1016/j.ijheatmasstransfer.2004.01.013.
[39] C.L. Bielders, L.W. De Backer, B. Delvaux, Particle density of volcanic soils as measured with a gas pycnometer, Soil Sci. Soc. Am. J. 54 (1990) 822, https://doi.org/10.2136/sssaj1990.03615995005400030034x.
[40] F. Liu, J. Wang, X. Qian, Integrating phase change materials into concrete through microencapsulation using cenospheres, Cem. Concr. Compos. 80 (2017) 317–325, https://doi.org/10.1016/j.cemconcomp.2017.04.001.
[41] A.M. Thiele, Z. Wei, G. Falzone, B.A. Young, N. Neithalath, G. Sant, et al., Figure of merit for the thermal performance of cementitious composites containing phase change materials, Cem. Concr. Compos. 65 (2016) 214–226, https://doi.org/10.1016/j.cemconcomp.2015.10.023.
[42] A.N. Norris, A.J. Callegari, P. Sheng, A generalized differential effective medium theory, J. Mech. Phys. Solids 33 (1985) 525–543, https://doi.org/10.1016/0022-5096(85)90001-8.
[43] R. Pal, Thermal conductivity of three-component composites of core-shell particles, Mater. Sci. Eng., A 498 (2008) 135–141, https://doi.org/10.1016/j.msea.2007.10.123.
[44] Y.M. Lee, R. Yang, Bin, Gau SS. A generalized self-consistent method for calculation of effective thermal conductivity of composites with interfacial contact conductance, Int. Commun. Heat Mass Transfer 33 (2006) 142–150, https://doi.org/10.1016/j.icheatmasstransfer.2005.10.004.
[45] E.P. Kearsley, P.J. Wainwright, Effect of porosity on the strength of concrete, Cem. Concr. Res. 32 (2002) 233–239.